Journal of Power Sources 246 (2014) 621–628

Contents lists available at ScienceDirect

Journal of Power Sources

journal homepage: www.elsevier.com/locate/jpowsour

Review

Polypyrrole/hexadecylpyridinium chloride-modified graphite oxide composites: Fabrication, characterization, and application in supercapacitors

Huixia Feng [a,*], Bin Wang [a], Lin Tan [a], Nali Chen [a], Nuoxin Wang [b,c], Baiyi Chen [a]

[a] College of Petrochemical Technology, Lanzhou University of Technology, Lanzhou 730050, PR China
[b] School of Life Science and Technology, Harbin Institute of Technology, Harbin 150080, PR China
[c] CAS Key Lab of Biological Effects of Nanomaterials and Nanosafety, National Center of Nanoscience and Technology, Beijing 100190, PR China

HIGHLIGHTS

- A facile method for synthesizing PPy/MGO composites by in situ polymerization.
- Observation of the markedly morphological distinction between PPy/GO and PPy/MGO.
- Excellent electrochemical performance of PPy/MGO composites.
- Excellent cycle stability and energy performance of PPy/MGO composites.

ARTICLE INFO

Article history:
Received 30 April 2013
Received in revised form
29 July 2013
Accepted 1 August 2013
Available online 28 August 2013

Keywords:
Polypyrrole
Graphite oxide
Supercapacitors
Modification

ABSTRACT

We report a facile and effective method for synthesizing polypyrrole/modified graphite oxide (PPy/MGO) composites by in situ polymerization. The graphite oxide (GO) is modified with hexadecylpyridinium chloride (CPC) and then composited with PPy. Scanning electron microscopy (SEM), X-ray diffraction (XRD), and Fourier transform infrared spectroscopy (FTIR) results demonstrate that PPy chains may combine with CPC molecule via π–π stacking interaction and the structures of PPy/GO and PPy/MGO composites are completely different. Cyclic voltammetry (CV), galvanostatic charge–discharge (GCD), and electrochemical impedance spectrum (EIS) tests indicate that, at the current density of 1 A g^{-1}, the specific capacitance and energy density of PPy/MGO are 202 F g^{-1} and 8.49 Wh kg^{-1} in three-electrode systems and those are 87 F g^{-1} and 10 Wh kg^{-1} in two-electrode systems; the capacitance retention of PPy/MGO is 83.8% after 1000 cycles at a scan rate of 1 A g^{-1}; PPy/MGO also exhibited excellent energy performance from Ragone charts. Based on these properties, the PPy/MGO composites may become a promising material for supercapacitor applications.

Crown Copyright © 2013 Published by Elsevier B.V. All rights reserved.

1. Introduction

Recently, graphite oxide (GO) has attracted extensive attention for its unique structure and properties. GO sheets possess not only a number of hydroxyl and epoxide functional groups anchored onto the surface sp^3-hybridized carbon atoms, but also considerable quantities of sp^2-hybridized carbon atom-containing carboxyl and carbonyl groups at their sheetedges [1]. Thus, GO has high dispersity in water [1,2]. Moreover, these carboxyl and carbonyl groups act as active spots, providing GO sheets strong reactivity with surfactant and polymers. These make it easy to fabricate GO-based composites.

Conducting polymers, featured with their relatively low cost, high environmental stability, high conductivity in doped state, high voltage window and so forth, are frequently-used materials for supercapacitors [3]. Unfortunately, swelling and shrinking of conducting polymers occur during the charge/discharge process, leading to electrochemical performance decline of conducting polymers during cycling. As a result, many conducting polymer-based composites are prepared to overcome this problem [4].

Polypyrrole (PPy), as one of the most significant conducting polymers, has been widely used in electronic devices, biomedical

* Corresponding author. Tel.: +86 136 7943 2853.
E-mail addresses: fenghx66@163.com, jeasonbin@163.com (H. Feng).

0378-7753/$ – see front matter Crown Copyright © 2013 Published by Elsevier B.V. All rights reserved.
http://dx.doi.org/10.1016/j.jpowsour.2013.08.002

devices, sensors, and other fields due to its good conductivity, thermal and photo stability in air [5]. Since PPy also tends to swell and shrink in cycling, many PPy/GO composites have been fabricated to pledge high performance when used for supercapacitors [6]. For instance, Yang et al. fabricated PPy/GO composites by direct electrochemical reduction process and demonstrated its enhanced specific capacity of 55 mAh g^{-1} at high 20 C rate (74% of that obtained at 1 C rate) without capacity fade during 200 charge/discharge cycles at 10 C rate [7]; Li et al. fabricated PPy nanowire/GO composites via in situ polymerization and the introduction of the PPy nanowire dramatically improved the specific capacity to 728 F g^{-1} at a discharge current density of 0.5 A g^{-1} and the specific capacitance retention to 93% after 1000 cycles at a scan rate of 50 mV s^{-1} [8].

Recently, an emerging idea in supercapacitor field has been reported that using the surfactant as the modifier will facilitate the formation of the conducting polymer/GO composites with excellent electrocapacitive performance [9]. Hitherto, however, the ultilization of CPC, a widely used cationic surfactant, as the modifier in the composition of PPy and GO has never been reported to the best of our knowledge. On the other hand, previous research in conducting polymer/surfactant-modified GO composites has focused on the increase of the conductivity and thermal stability of the composites, but little attention has been given to the effect of surfactant-modified GO on the structure and electrochemical performance of the composites [9].

In this paper, we report a novel method to synthesize PPy/MGO composites. MGO was prepared by the self-assembly of CPC on the surfaces of GO and then the composites were synthesized in MGO suspension containing dispersed pyrrole (Py) monomer with an in situ polymerization method. After the examination of the structure and electrochemical performance of the composites, we proved its unique structure, high specific capacitance, high capacitance utilization, excellent cycle stability and excellent energy performance. These properties indicate that the as-prepared PPy/MGO composites may become a promising candidate in supercapacitor field.

2. Experimental section

2.1. Materials

Graphite powder (325 mesh) was purchased from Kaitong Co. LtD. (Tianjin, China). Py monomer was purified by distillation under reduced pressure before use. Other reagents were commercially available and of analytical reagent grade. All solutions were prepared with distilled water.

2.2. Preparation of GO and MGO

GO was prepared from natural graphite via a modified Hummers method [10]. Firstly, preoxidized graphite powder was synthesized through reaction of natural graphite (3 g), sulfuric acid (12 mL), $K_2S_2O_8$ (2.5 g), and P_2O_5 (2.5 g). The reaction mixture was maintained at 80 °C for 5 h and terminated by adding 500 mL deionized water. This preoxidized graphite powder (600 mg) was further oxidized by sulfuric acid (24 mL) and $KMnO_4$ (3 g), and maintained at room temperature for 2 h and then at 35 °C for 2 h. After that, the reaction mixture was maintained at 98 °C for 0.5 h and terminated by adding 50 mL deionized water. After the dilution with deionized water (150 mL) and decomposition of excessive $KMnO_4$ by H_2O_2 (30 wt%, 6 mL), the resulting GO solution was filtered and washed with deionized water for 3 times, and removed metal ions by dialysis membranes for a week. GO film was obtained after drying in a vacuum for 24 h. Following sonication the GO aqueous media for 1 h, CPC (the mass ratio of CPC and GO was 0.03) was added and MGO solution was prepared by magnetic stirring for 1 h.

2.3. Preparation of PPy

PPy was prepared by chemical oxidation. 1 mL Py monomer was dispersed in 50 mL distilled water at ambient temperature. Then, under nitrogen protection, 0.8148 g sulfamic acid (SA) and 50 mL 0.3 M $FeCl_3$ solution was added slowly to the mixture. After magnetic stirring for 0.5 h, the resultant product was dried under vacuum at 40 °C for 12 h to obtain a black powder of PPy.

2.4. Preparation of PPy/GO and PPy/MGO composites

GO (38.7 mg) was added into 50 mL deionized water and sonicated for 1 h to get colloidal GO, followed by the addition of 200 μL pyrrole monomer and 163 mg SA. The mixture was stirred at room temperature for 1 h and then 50 mL 0.06 M $FeCl_3$ solution were added slowly to the above suspension under nitrogen protection for 0.5 h for in situ polymerization of PPy. The resultant product was dried under vacuum at 40 °C for 12 h to obtain a black powder of PPy/GO composites. The preparation of PPy/MGO composites was the same as the process of PPy/GO except that GO was replaced by MGO.

2.5. Structure characterization

The morphology of PPy/MGO composite was observed by a JSM-6701F field emission SEM. The sample was mounted on a metal stub and coated with gold before observation. The molecular structure of the composite was identified by IR spectroscopy on a Nicolet AVTAR 360 FTIR spectrophotometer using KBr pellets. XRD analysis was conducted on a powder Shimadzu-XRD6000 diffractometer with CuKα radiation.

2.6. Electrochemical tests

The test electrodes were prepared by mixing the samples, acetylene black, and graphite in the mass ratio of 8:1:1, followed by adding 10 μL polytetrafluoroethylene and 50 μL ethanol in the above mixture and grinding adequately to form a slurry. The slurry was coated onto a surface of nickel foam, dried under vacuum at 60 °C for 24 h and then compressed at 10 MPa for 5 min. All electrochemical experiments were carried out in 2 M $NaNO_3$ solution. In a three-electrode system, platinum foils and saturated calomel electrode were used as counter and reference electrodes; in a two-electrode system, the counter electrode also acted as the reference electrode using the same materials as the working electrode. CV, EIS, and GCD measurements were performed with a CHI660D workstation. CV tests were conducted between −0.4 and 0.7 V at a rate of 10 mV s^{-1}. EIS measurements were performed in the frequency range from 10^5 to 10^{-2} Hz at an open circuit potential with an AC perturbation of 5 mV. GCD curves were measured at a current density of 1 A g^{-1}. The voltage windows of CV and GCD tests were set in the range from −0.4 to 0.7 V in the three-electrode system and from 0 to 1 V in the two-electrode system.

2.7. Measurement of conductivity

For the measurement of conductivity, all test samples were prepared in pellet form (diameter: 13 mm, thickness: 0.6 mm) at pressure of 40 MPa. Four probes method was used to measure the conductivity of the obtained sample by a four-probe resistivity/

square resistance tester (Kund Technology Co. Ltd., Guangzhou, China).

3. Results and discussion

3.1. Structure characterization

The morphology of the structure of PPy, GO, PPy/GO, and PPy/MGO were characterized by SEM firstly. As shown in Fig. 1, PPy exhibits A globular submicron structure with diameters ranging between 100 and 300 nm, and GO exhibits a layered structure and its sheets fold onto themselves resulting in a wrinkled surface (Fig. 1 PPy, GO). Many PPy particles with short rods distribute on the surface of PPy/GO (Fig. 1 PPy/GO (a)), which indicates PPy morphology is changed with the introduction of GO. However, many PPy particles with globulars are on the surface of PPy/MGO (Fig. 1 PPy/MGO (a)) and this indicates PPy morphology keeps almost unchanged with the introduction of MGO. In the meantime, GO sheets become closer to each other in PPy/GO composite (Fig. 1 PPy/GO (b)), while, they are peeled in PPy/MGO composite (Fig. 1 PPy/MGO (b)). These huge changes in morphology indicate that the introduction of CPC play an important role in adjusting the surface shape in the preparation process.

The XRD spectra of the as-prepared GO, PPy, PPy/GO, and PPy/MGO are presented in Fig. 2a. The original diffraction peak of the natural graphite at 26.3° disappears after oxidation treatment, and a sharp peak at 11.3° is detected, which is attributed to the oxygen-containing functional groups and water molecule insertion between the GO layers [11]. In addition, it is noted that a small peak appears at 24.2°, suggesting unoxidized graphitic domains. By comparison, in PPy/GO samples, the characteristic peak of GO disappears and the characteristic peak of unoxidized graphitic domains moves a little bit forward; in PPy/MGO samples, the presence of PPy characteristic peak is obvious, just moving from 21.8° to 21.4° (Fig. 2).

All the above observations indicate that crystallite structure of PPy/GO is similar to GO, while that of PPy/MGO is similar to PPy. These may be attributed to different polymerization processes of Py monomer when CPC are introduced (see also the proposed formation mechanism in Section 3.2 and Scheme 1).

We also performed FTIR examination on GO, PPy, PPy/GO, and PPy/MGO (Fig. 2b). The spectrum for GO shows a broad and intense O–H peak at 3437 cm^{-1}. Other peaks are assigned as follows: C=O peak in carboxylic acid and carbonyl moieties at 1735 cm^{-1}, C–O–C peak at 1399 cm^{-1}, and C–O stretching peak at 1081 cm^{-1}. The peak at 1621 cm^{-1} may be attributed to skeletal vibrations of unoxidized graphitic domains [12]. In the spectrum of PPy, the peaks at 1530 and 1453 cm^{-1} are assigned to C=C and C–C stretching, respectively. Meanwhile, the peaks at 1294 and 1030 cm^{-1} correspond to =C–H band in plane vibration; the peaks at 1156 cm^{-1} are ascribed to N–C stretching; the peaks at 899 cm^{-1} are assigned to the =C–H out of plane vibration, indicating polymerization of pyrrole. The spectra of the PPy/GO and PPy/MGO composites illustrate the obvious presence of PPy characteristic vibrations, because the peaks at 1156 cm^{-1} assigned to the N–C stretching of PPy in these two composites are moved to 1164 and 1177 cm^{-1}, respectively. In addition, it is noticed that a new peak appears at around 1640 cm^{-1} in PPy/GO and PPy/MGO samples, which corresponds to skeletal vibrations of unoxidized graphitic domains. These indicated that PPy can be successfully deposited on the GO surface and interactions were present between GO and PPy in the composites.

3.2. Formation mechanism

Proposed possible formation processes of PPy/GO and PPy/MGO composites are shown in Scheme 1. Under sonication, GO is exfoliated into graphene oxide and stably dispersed in water. When a large amount of Py is added to GO aqueous solution, many Py molecules combine with electroactive functional groups of GO via hydrogen bonding. As the oxidant $FeCl_3$ is added, the polymerization process happens on the surface of GO and the PPy chains firmly attach to the surface of GO, so crystallite structure of PPy/GO is similar to GO. In contrast, if GO is modified with CPC, the hydrogen atoms of functional groups of GO are replaced by CPC molecules

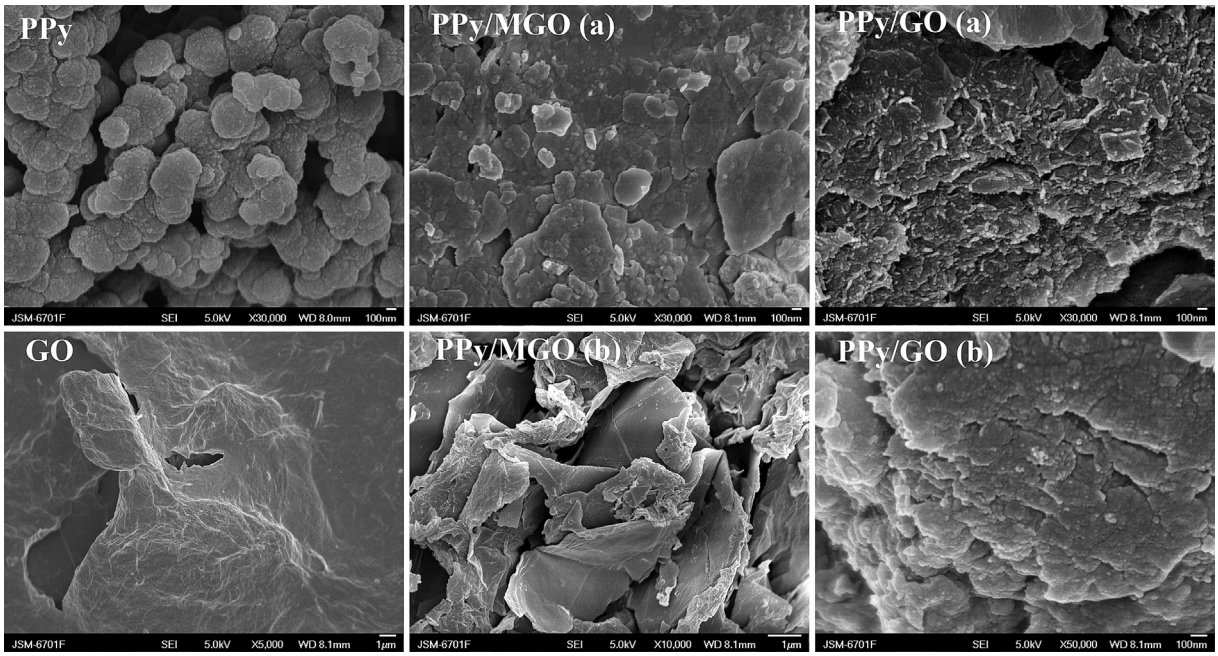

Fig. 1. SEM images of PPy, GO, PPy/GO, and PPy/MGO. PPy/GO (a) and PPy/MGO (a) show the surface topography of the two composites; PPy/GO (b) and PPy/MGO (b) show the interlayer appearance of both composites.

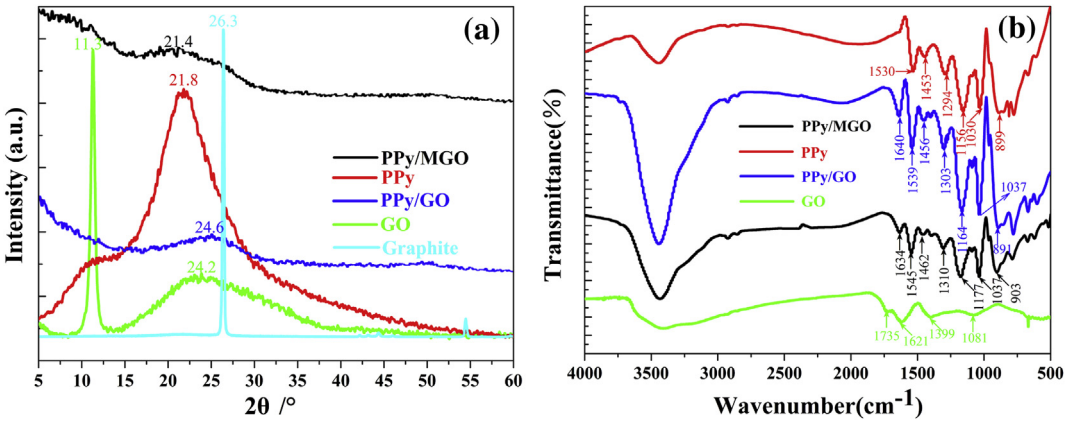

Fig. 2. (a) XRD patterns for graphite, GO, PPy, PPy/GO, and PPy/MGO; (b) FTIR spectra of GO, PPy, PPy/GO, and PPy/MGO.

and hydrophobic groups (pyridine rings) of CPC are directionally arranged in aqueous solution. Here, CPC molecules act three roles: firstly, they occupy the functional groups for Py molecules to combine with GO; secondly, pyridine rings prevent Py molecules from contacting with functional groups of GO; finally, directional arrangement of pyridine rings in aqueous solution facilitates layer peeling of GO. In this case, the polymerization process happens in GO aqueous solution and PPy chains combine with pyridine rings of CPC molecule via π−π stacking interaction on the surface of GO, so crystalline structure of PPy/MGO is similar to PPy.

3.3. Electrochemical performance of the electrodes (three-electrode system)

We tested the electrochemical performance of the samples in a three-electrode system. Fig. 3a shows CV curves of the pure systems and the composites, at a scan of 10 mV s^{-1} between −0.4 and 0.7 V in 2 M $NaNO_3$ aqueous media. The as-prepared composites and PPy demonstrate typical capacitive behaviors with quasi-rectangular profiles. The CV curve of PPy/MGO is closer to a rectangle in shape compared with PPy and PPy/GO at the same scan rate, indicating the better electrochemical performance [13]. Moreover, it can be observed that the larger current response of the PPy/MGO corresponds to a higher specific capacitance, compared with PPy, PPy/GO, and GO. This is because conductivity of PPy/MGO (22.22 S cm^{-1}) is higher than PPy/GO (12.50 S cm^{-1}) and PPy (17.54 S cm^{-1}). It is known that the poor electrochemical performance of GO results from their poor electrical conductivity and low faradic reaction rate [14]. But conductivity of composites depends on both conductivity of each component of composites and space structure of composites [15]. We can see conductivity of PPy/GO is lower than PPy, due to not only the poor conductivity of GO, but

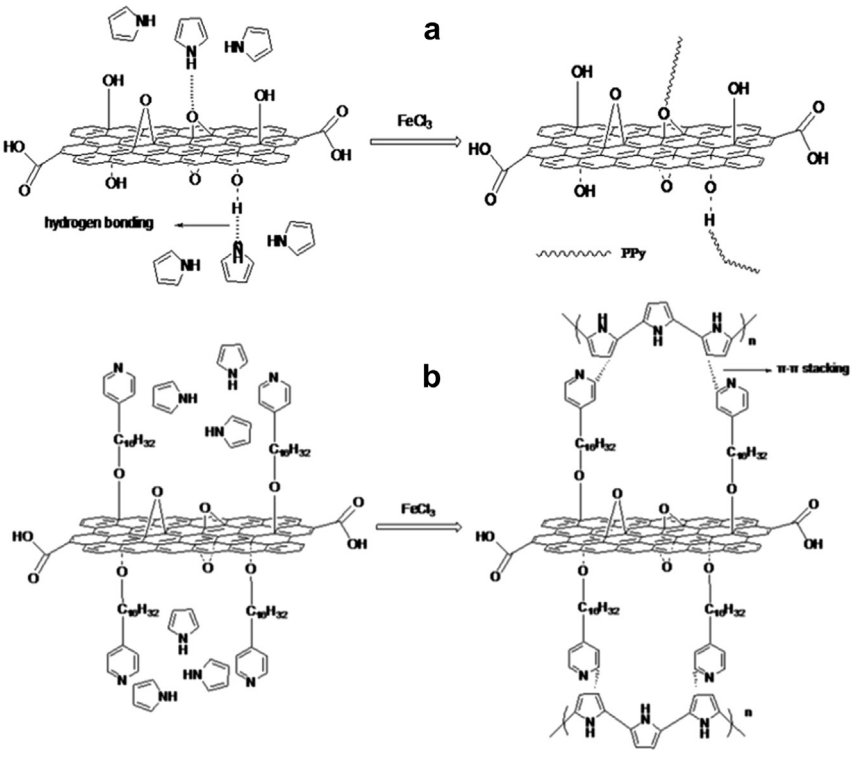

Scheme 1. Proposed possible combining modes of PPy/GO (a) and PPy/MGO (b) composites.

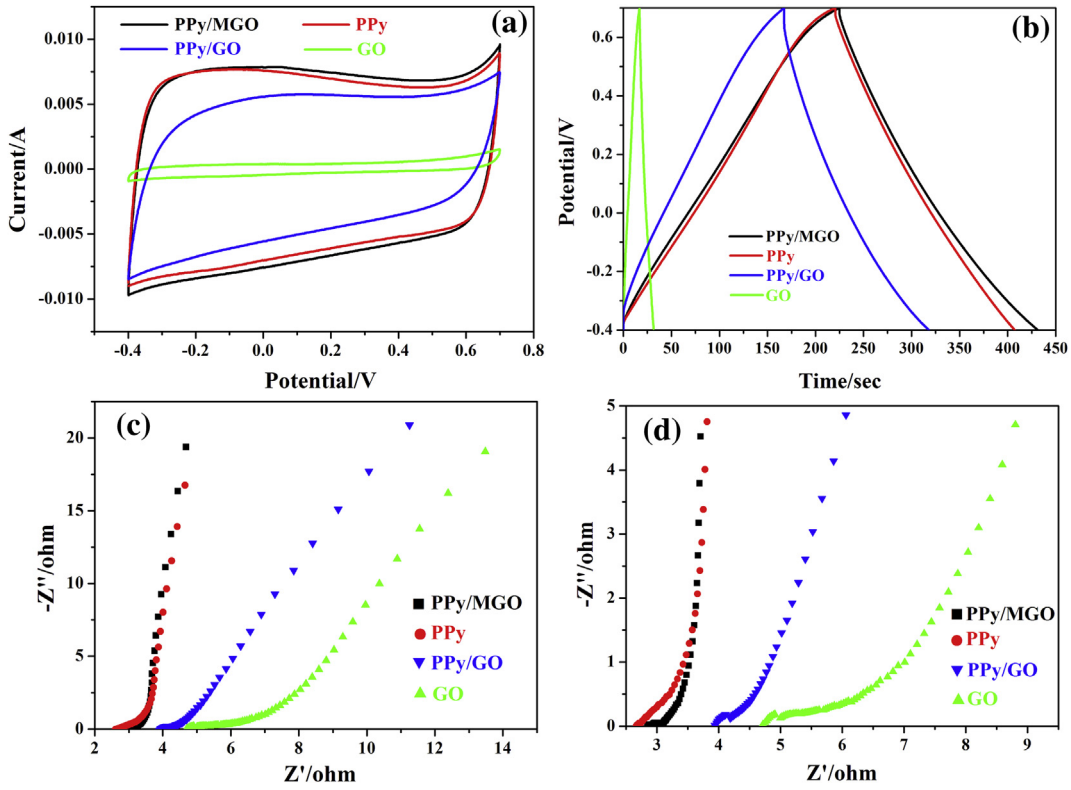

Fig. 3. Electrochemical characterization for GO, PPy, PPy/GO, and PPy/MGO in a three-electrode system. (a) CV curves for PPy/MGO, PPy, PPy/GO, and GO at a scan rate of 10 mV s^{-1}; (b) Galvanostatic charge–discharge curves for PPy/MGO, PPy, PPy/GO, and GO at a constant current density of 1 A g^{-1}; (c) Nyquist plots for PPy/MGO, PPy, PPy/GO, and GO; (d) Amplified Fig. 3c on the region of high frequency.

also the firm attachment of PPy chain to the surface of GO which reduces the connection between PPy chains. Meanwhile, conductivity of PPy/MGO is higher than PPy. This is because PPy chains attach to surfaces of MGO though π–π stacking interaction between PPy chains and pyridine rings of CPC molecules, thereby increasing the connection between PPy chains, facilitating the formation of the space conductive network. From the SEM image in Fig. 1, we can infer that peeled GO sheets result in the distance decrease for the electron shuttling in PPy/MGO composites. Furthermore, the huge surface area of PPy/MGO composites increases the reaction area during the electrochemical reaction.

The specific capacitances (C_m) of the prepared samples can be calculated from the GCD curves (Fig. 3b) using the following equation:

$$C_m = \frac{I \times t}{\Delta V \times m} \quad (1)$$

where I, t, ΔV, and m denote the current during discharge, discharge time, potential drop during the discharge progress, and the mass of the active material, respectively [16]. From Eq. (1), the specific capacitances of PPy/MGO, PPy, PPy/GO, and GO are found 202, 170, 137, and 13 F g^{-1}, respectively. Meanwhile, the capacitance utilization of the PPy in the composites ($C_{m,\,PPy}$) can be calculated using the following equation:

$$C_{m,PPy} = \frac{C_{m,electrode} - (1 - W_{PPy})C_{m,GO}}{W_{PPy}} \quad (2)$$

where $C_{m,electrode}$, W_{PPy}, and $C_{m,GO}$ denote the specific capacitance of the composite electrode, weight fraction of PPy in the composites, and specific capacitance of the GO electrode, respectively. From Eq. (2), the capacitance utilization of PPy in PPy/MGO and PPy/GO are found to be 183 and 129 F g^{-1}, respectively. The capacitance utilization of PPy in PPy/GO is lower than that of pure PPy, instead, in PPy/MGO is higher, indicating a synergistic effect between MGO and PPy in PPy/MGO. High loading and homogeneous distribution of PPy on MGO surfaces are advantageous for MGO sheets to transport ions in the pore system and increasing the PPy-electrolyte interfacial area. This is supported by the SEM and XRD results.

EIS is complementary to galvanostatic cycling measurements, which will provide more information on the electrochemical frequency behavior of the system. The more vertical the curve, the more closely the supercapacitor behaves as an ideal capacitor [17]. It can be seen that the slope of the straight line in the low-frequency of the PPy/MGO is larger than the others, which evidently indicated that the PPy/MGO composite have better supercapacitor behavior than the others (Fig. 3c). From the point intersecting with the real axis in the region of high frequency, internal resistance (R_s) can be obtained. The internal resistance is related to several parameters: the ionic resistance of the electrolyte, the intrinsic resistance of the active material, and the contact resistance at the interface active material [18]. The semicircle diameter in the region of high frequency implies the charge transfer resistance [18]. As shown in Fig. 3d, the enlarged view of Fig. 3c in the region of high frequency, the internal resistance of PPy/MGO, PPy/GO, PPy, and GO are about 2.8, 3.9, 2.7, and 4.7 Ω, respectively. This indicates that the internal resistance of PPy/MGO is lower than that of PPy/GO. Furthermore, the semicircle diameter of PPy/MGO composite is much lower than the other materials, suggesting its lower charge-transfer impedance (Fig. 3d). The 45° region

(Warburg region) is a consequence of the frequencies dependence of ion diffusion in the electrolyte to the electrode interface. In Fig. 3c, the Warburg curve of PPy/MGO composites is considerably short for its short ion diffusion path, which facilitates the efficient access of electrolyte ions to the electrode surface [19].

Also, the performance of supercapacitors commonly requires a power density substantially greater than batteries with acceptably high energy densities in order to resist self-discharge, and hence a high time constant value is necessary. Energy density (E) and the maximum power density (P) of PPy/MGO and PPy/GO are calculated from the following equations:

$$E = \frac{C(\Delta V)^2}{7.2} \tag{3}$$

$$P = \frac{E \times 3600}{\Delta t} \tag{4}$$

where E, C, ΔV, P, and Δt are energy density, total specific capacitance (1/4 of the single electrode capacitance [20]), potential window of discharge, power density, and the time spent in discharge, respectively [16b,20,21]. Energy density and maximum power density of PPy/MGO are 8.49 Wh kg^{-1} and 149.1 W kg^{-1}, while those for PPy/GO are 5.76 Wh kg^{-1} and 136.69 W kg^{-1}. The PPy/MGO composites electrode demonstrates a much higher energy density than conventional capacitors [16b]. Besides, the value of power density is well-suited for fabricating supercapacitor devices as well [22].

3.4. Symmetric surpercapacitors performance (two-electrode system)

A two-electrode system is often used to evaluate the applicability of the potential surpercapacitor materials. The CV (Fig. 4a), GCD (Fig. 4b), and EIS (Fig. 4c and d) graphs in two-electrode systems confirm the excellent electrochemical performance of PPy/MGO from the three-electrode system. We also calculated the characteristic parameters of the two-electrode systems from Eqs. (5)–(7). All data reveal the better performance of PPy/MGO, except of the slight decrease in energy density. Based on Fig. 4a, the specific capacitance in two-electrode systems was carried out according to the following equation:

$$C_g = \frac{I \times \Delta t}{\Delta V \times m} \tag{5}$$

where I, Δt, ΔV, and m denote the applied discharge current, the discharged time after IR drop, the discharge potential window after IR drop, and the mass of the total mass of the two electrode materials, respectively [23]. C_g values of PPy/MGO, PPy, and PPy/GO are found 87, 74, and 58 F g^{-1}, respectively.

Likewise, energy density (E_g) and the maximum power density (P_g) of PPy/MGO and PPy/GO are calculated from the following equations:

$$E_g = \frac{C_g \Delta V^2}{7.2} \tag{6}$$

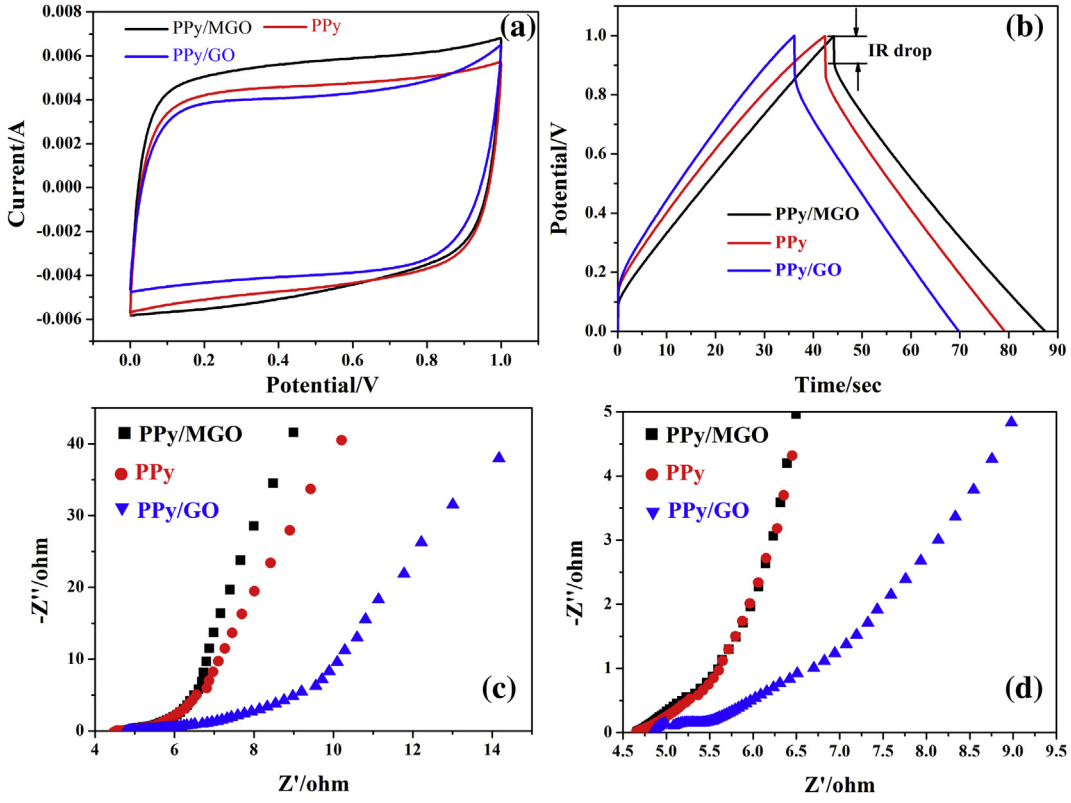

Fig. 4. Electrochemical characterization for GO, PPy, PPy/GO, and PPy/MGO in a two-electrode system. (a) CV curves for PPy/MGO, PPy, and PPy/GO at a scan rate of 10 mV s^{-1}; (b) GCD curves for PPy/MGO, PPy, and PPy/GO, at a constant current density of 1 A g^{-1}; (c) Nyquist plots for PPy/MGO, PPy, and PPy/GO; (d) Amplified Fig. 4c on the region of high frequency.

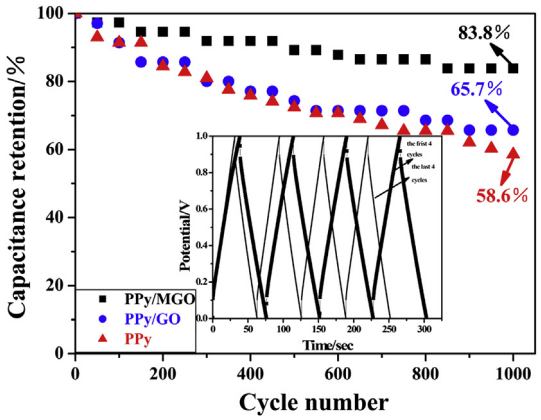

Fig. 5. Percentage retention of the specific capacitance as a function of charge–discharge cycles at a constant current density of 1 A g^{-1} in a two-electrode system. The inset shows the charge–discharge curves of the first and last 4 cycles for PPy/MGO.

$$P_g = \frac{E_g \times 3600}{t} \quad (7)$$

where ΔV, t, E_g, and P_g denote the discharge potential window after IR drop, the discharged time after IR drop, the energy density, and the power density, respectively [24]. From Eqs. (6) and (7), the energy density and power density of PPy/MGO are 10 Wh kg^{-1} and 825 W kg^{-1}, while those of PPy/GO are 7.5 Wh kg^{-1} and 850 W kg^{-1}. From Fig. 4d (the enlarged view of Fig. 4c in the region of high frequency), the internal resistance of PPy/MGO, PPy, and PPy/GO are 4.6, 4.6, and 4.8 Ω, respectively. In addition, it is clearly seen that the curves of PPy/MGO and PPy are essentially coincident. The results suggest that PPy/MGO and PPy have almost the same capacitor behavior in the high frequency and this consistency links to the similarity in their morphology.

The cycle stability of the prepared samples was evaluated by repeating the GCD test in the two-electrode system (Fig. 5). The specific capacitance of PPy/MGO shows a 16.2% variation after as many as 1000 cycles, considerably smaller than that of the PPy/GO (34.3%) and PPy (41.4%). These are illustrations of excellent cycling stability and reversibility in the repetitive cycling for PPy/MGO.

Fig. 6 shows the Ragone plot of the corresponding power and energy densities for the PPy/MGO and PPy. The energy densities of PPy/MGO and PPy are 12.6 and 10.82 Wh kg^{-1} obtained at 0.25 A g^{-1} (with power density of 244 and 234.4 W kg^{-1} at this point), respectively. Additionally, for PPy/MGO, an energy density of 8.21 Wh kg^{-1}, about 1.5 times higher than that of PPy (with power density of 5.47 Wh kg^{-1} at this point), was achieved at the current density of 1.5 A g^{-1}. The results indicate that PPy/MGO has significantly better energy performance than PPy.

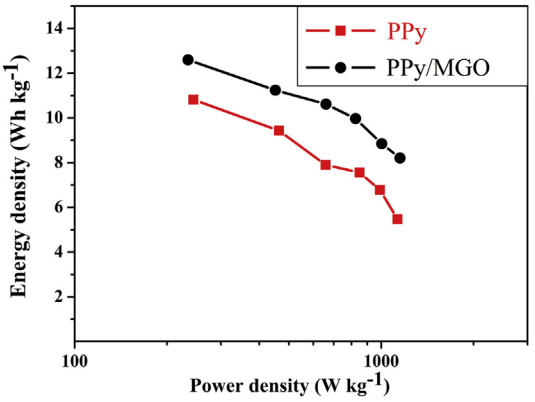

Fig. 6. Ragone plots for PPy/MGO and PPy in a two-electrode system.

4. Conclusion

In summary, we have developed a facile and effective approach to synthesize PPy/MGO composites. The crystalline structure of PPy/MGO is similar to PPy, but that of PPy/GO resembles GO. Notably, the PPy/MGO composites electrode has demonstrated superior performance: (1) In three-electrode systems, the specific capacitance of PPy/MGO (202 F g^{-1}) is higher than those of pure PPy (170 F g^{-1}) and PPy/GO (137 F g^{-1}); the capacitance utilization of PPy in PPy/MGO (183 F g^{-1}) is higher than that of pure PPy (170 F g^{-1}) and PPy/GO (129 F g^{-1}). (2) In two-electrode systems, the specific capacitance of the whole cell for PPy/MGO (87 F g^{-1}) is much higher than PPy/GO (58 F g^{-1}) at 1 A g^{-1}. (3) It can work at a high energy density of 149.1 W kg^{-1}, a much higher energy density than conventional capacitors. (4) PPy/MGO possesses excellent capacitance retention of is 83.8% after 1000 cycles at a scan rate of 1 A g^{-1}, considerably higher than those of PPy/GO (65.7%) and PPy (58.6%). (5) PPy/MGO has a much better energy performance than the PPy. These features suggest an excellent potential composite in the use of supercapacitors.

Acknowledgments

This work was financially supported by the National Natural Science Foundation of China (No. 51063003) and the Fundamental Research Funds for the Universities of Gansu (No. 1105ZTC136).

References

[1] Y.Q. Han, B. Ding, X.G. Zhang, Chi. Sci. Bull. 56 (2011) 2846–2852.
[2] (a) C. Hontoria-Lucas, A.J. López-Peinado, J. de D. López-González, M.L. Rojas-Cervantes, R.M. Martín-Aranda, Carbon 33 (1995) 1585–1592;
(b) T. Szabó, E. Tombácz, E. Illés, I. Dékány, Carbon 44 (2006) 537–545.
[3] G.P. Wang, L. Zhang, J.J. Zhang, Chem. Soc. Rev. 47 (2012) 797–828.
[4] (a) X.J. Lu, H. Dou, C.Z. Yuan, S.D. Yang, L. Hao, F. Zhang, L.F. Shen, L.J. Zhang, X.P. Zhang, J. Power Sources 197 (2012) 319–324;
(b) H.F. An, Y. Wang, X.Y. Wang, L.P. Zheng, X.Y. Wang, L.H. Yi, L. Bai, X.Y. Zhang, J. Power Sources 195 (2010) 6964–6969.
[5] J.W. Kim, F. Liu, H.J. Choi, S.H. Hong, J. Joo, Polymer 44 (2003) 289–293.
[6] L.L. Zhang, S.Y. Zhao, X.N. Tian, X.S. Zhao, Langmuir 26 (2010) 17624–17628.
[7] Y. Yang, C.Y. Wang, B.B. Yue, Sanjeev Gambhir, Chee O. Too, Gordon G. Wallace, Adv. Energy Mater. 2 (2012) 266–272.
[8] J. Li, H.Q. Xie, Y. Li, J. Power Sources 241 (2013) 388–395.
[9] L.L. Zhang, S.Y. Zhao, X.N. Tian, X.S. Zhao, Langmuir 22 (2010) 17624–17628.
[10] (a) H.F. Yang, Q.X. Zhang, C.S. Shan, F.H. Li, D.X. Han, L. Niu, Langmuir 26 (2010) 6708–6712;
(b) Y.-J. Park, S.Y. Park, I. In, J. Ind. Eng. Chem. 17 (2011) 298–303.
[11] (a) D. Nandi, K. Gupta, A.K. Ghosh, A. De, S. Banerjee, U.C. Ghosh, J. Nanopart. Res. 14 (2012) 1–14;
(b) D.Y. Pan, S. Wang, B. Zhao, M.H. Wu, H.J. Zhang, Y. Wang, Z. Jiao, Chem. Mater. 21 (2009) 3136–3142.
[12] (a) S. Stankovich, R.D. Piner, S.T. Nguyen, R.S. Ruo&fflig, Carbon 44 (2006) 3342–3347;
(b) Y.X. Xu, H. Bai, G.W. Lu, G.Q. Shi, J. Am. Chem. Soc. 130 (2008) 5856–5857.
[13] D.C. Zhang, X. Zhang, Y. Chen, P. Yu, C.H. Wang, Y.W. Ma, J. Power Sources 196 (2011) 5990–5996.
[14] H.P. Yang, J. Jiang, W.W. Zhou, L.F. Lai, L.F. Xi, Y. Lam, Z.X. Shen, B. Khezri, T. Yu, Nanoscale Res. Lett. 130 (2011) 531–538.
[15] H. Zhang, X. Zhong, J.J. Xu, H.Y. Chen, Langmuir 24 (2008) 13748–13752.
[16] (a) S.H. Cho, J.S. Joo, B.R. Jung, T.M. Ha, J.Y. Lee, Macromol. Res. 17 (2009) 746–749;
(b) J.F. Zang, X.D. Li, J. Mater. Chem. 21 (2011) 10965–10969;
(c) H.L. Wang, Q.L. Hao, X.J. Yang, Nanoscale 2 (2010) 2164–2170.
[17] L.F. Lai, H.P. Yang, L. Wang, B.K. Teh, J.Q. Zhong, H. Chou, L.W. Chen, W. Chen, Z.X. Shen, R.S. Ruoff, J.Y. Lin, ACS Nano 6 (2012) 5941–5951.
[18] J. Zhang, Y. Yu, L. Liu, Y. Wu, Nanoscale 5 (2013) 3052–3057.
[19] R.I. Jaidev, A.K. Jafri, S. Mishra, J. Ramaprabhu, Mater. Chem. 21 (2011) 17601–17605.

[20] W. Xing, S.Z. Qiao, R.G. Ding, F. Li, G.Q. Lu, Z.F. Yan, H.M. Cheng, Carbon 44 (2006) 216–224.
[21] (a) S. Bose, T. Kuila, A.K. Mishra, R. Rajasekar, N.H. Kim, J.H. Lee, J. Mater. Chem. 22 (2012) 767–784;
(b) R.B. Rakhi, W. Chen, H.N. Alshareef, J. Mater. Chem. 22 (2012) 5177–5183.
[22] Y. Wang, Z.Q. Shi, Y. Huang, Y.F. Ma, C.Y. Wang, M.M. Chen, Y.S. Chen, J. Phys. Chem. C 113 (2009) 13103–13107.
[23] C.C. Xiang, M. Li, M.J. Zhi, A. Manivannan, N.Q. Wu, J. Mater. Chem. 22 (2012) 19161–19167.
[24] W.W. Liu, X.B. Yan, J.W. Lang, C. Peng, Q.J. Xue, J. Mater. Chem. 22 (2012) 17245–17253.